Growth of Porous Type Anodic Oxide Films at Micro-Areas on Aluminum Exposed by Laser Irradiation

Tatsuya Kikuchi[a,*], Masatoshi Sakairi[a], and Hideaki Takahashi[b]
[a]Graduate School of Engineering, Hokkaido University,
N13-W8, Kita-Ku, Sapporo, 060-8628, Japan
[b]Asahikawa National College of Technology,
Syunkohdai, 2-2, 1-6, Asahikawa, 071-8142, Japan

Abstract

Aluminum covered with pore-sealed anodic oxide films was irradiated with a pulsed Nd-YAG laser to remove the oxide film at micro-areas. The specimen was re-anodized for long periods to examine the growth of porous anodic oxide films at the area where substrate had been exposed by measuring current variations and morphological changes in the oxide during the re-anodizing. The chemical dissolution resistance of the pore-sealed anodic oxide films in an oxalic acid solution was also examined by measuring time-variations in rest potentials during immersion.

The resistance to chemical dissolution of the oxide film became higher with increasing pore-sealing time and showed higher values at lower solution temperatures. During potentiostatic re-anodizing at five 35-μm wide and 4-mm long lines for 72 h after the film was removed the measured current was found to increase linearly with time. Semicircular columnar shaped porous type anodic oxide was found to form during the re-anodizing at the laser-irradiated area, and was found to grow radially, thus resulting in an increase in the diameter. After long re-anodizing, the central and top parts of the oxide protruded along the longitudinal direction of the laser-irradiated area. The volume expansion during re-anodizing resulted in the formation of cracks, parallel to the lines, in the oxide film formed during the first anodizing.

Key words: Aluminum; Anodizing; Laser Irradiation; Micro-fabrication

1. INTRODUCTION

Porous type anodic oxide films on aluminum have been widely investigated in the field of surface finishing of aluminum in order to improve corrosion resistance and fabricate nanostructure. Specifically, highly ordered pore arrays in the oxide films have been used for the fabrication of nano-rods and nano-tubes of oxides, metals, and semiconductors as well as carbon nano-tubes [1-8]. In these investigations, the whole surface of the aluminum specimens is anodized in oxalic, sulfuric, or phosphoric acid solution, and the oxide films with highly ordered pore arrays are used as templates to form the nanostructures. If porous anodic oxide films are formed at selected areas by micro- and nano-patterning techniques, it would be possible to fabricate more

sophisticated nanostructures [9]. The localized formation and growth behavior of anodic oxide films, however, have received little investigation.

In previous investigations, the authors have reported on microstructure fabrication by aluminum anodizing, laser irradiation, and electrochemical techniques [10-19]. In these techniques, an aluminum plate or tube covered with porous type oxide films was irradiated with a pulsed Nd-yttrium aluminum garnet (YAG) laser to remove the oxide film, and then electroplate with metals such as Ni, Cu, Pt, and Au [10-13, 15, 17-19]. Similar techniques carried out at the laser-irradiated area have included electro-phoretic deposition of acrylic acid / melamine resin [13], electro-polymerization of polypyrrole [14, 16], and electrochemical etching of the aluminum substrate [12]. Three-dimensional (3D) microstructures, 3D micro-manipulators, printed circuit boards, micro-injection molds, and micro-electrochemical rectors were fabricated by applying the above techniques. Three-dimensional micropatterns can be fabricated by rotation and moving up and down of the 3D-shape aluminum specimen during laser irradiation. The laser irradiation technique combined with electrochemical techniques can achieve fabrication of 3D microstructures, whereas photolithography with photoresists/templates is less suitable for 3D structure fabrication.

In previous investigations, the authors found that porous type oxide films can be formed at a selected area by re-anodizing after the initial laser irradiation [12], although the growth behavior and mechanism were not investigated in detail. The present investigation reports the localized formation of porous type anodic oxide films on aluminum after laser-irradiation of insulating oxide film-covered substrates. The goal of the current investigation was to form the anodic oxide films on the aluminum substrate with high resistance to chemical dissolution in anodizing solutions, and to describe the growth behavior of the porous type oxide films at the selected-area by electrochemical measurements and morphological observations.

2. EXPERIMENTAL

2.1 Specimens and pretreatment

Highly pure aluminum plates (99.99 wt%, 0.40 mm thick, 30 mm x 20 mm, Nippon Light Metal Co.) were used as specimens. The specimens were ultrasonically degreased in a C_2H_5OH solution, and then electropolished in a 13.6 M CH_3COOH / 2.56 M $HClO_4$ solution with a constant voltage of 28 V at 280 K for 150 s. Electropolished specimens were anodized in 0.22 M $(COOH)_2$ solution at 293 K for 10 min with a constant current density of 100 A/m^2 to form porous type oxide films with 3 μm thicknesses. After anodizing, some specimens were boiled in doubly distilled water for t_p = 15 - 120 min (t_p: pore sealing time) to seal the pores in the oxide film.

2.2 Rest potential measurements of the anodized specimen in oxalic acid solution

The pore-sealed anodic oxide films remaining at areas not subjected to laser-irradiation, which act as insulating masks during re-anodizing in $(COOH)_2$

solution, are attacked by the re-anodizing solution. The exposure to a re-anodizing solution decreases in the thickness and causes the development of imperfections due to the slow dissolution of the oxide. This is possibly one cause of the pore-sealed oxide film losing the ability to act as masks after long periods of re-anodizing. To determine the optimal conditions for re-anodizing, the dissolution resistance of the pore-sealed oxide film in acid solution was examined by the following experiments.

Anodized and pore-sealed specimens with different t_ps were immersed in 0.22 M $(COOH)_2$ solution at T_i = 280 - 306 K (T_i: immersion temperature) for t_i = 24 h (t_i : immersion time), and the time-variations in the rest potential of the specimens, E_r, vs. t_i were measured during immersion. A saturated KCl-Ag/AgCl electrode was used as the reference electrode.

2.3 Localized removal of the anodic oxide film by laser irradiation

Anodized and pore-sealed specimens were immersed in doubly distilled water at 295 K, and then irradiated with a pulsed Nd-YAG laser. Details of the laser irradiation setup have been shown elsewhere [13]. The specimens were set in the focal position of a laser beam that had passed through a beam splitter, an iris diaphragm, a convex lens with 60 mm focal length, and a quartz window. The laser beam has a 532 nm wavelength (second harmonic generation), 8 ns pulse width, 10 Hz frequency, and < 0.5 mrad. beam divergence (full angle), and the laser power was adjusted to P = 1.0 mW. The specimens were moved at 33 μm/s with a PC-controlled XY-stage during the laser irradiation, and 5 straight lines of removed oxide film of 4 mm length and at 1 mm intervals were fabricated by laser irradiation of the specimens. The width of the lines was 35 μm as described in the results and discussion section.

2.4 Re-anodizing of the laser-irradiated specimens

After the laser-irradiation, the specimens were again immersed in 0.22 M $(COOH)_2$ solution at 280 K, and then re-anodized for 72 h to form porous type oxide at the laser-irradiated area. During re-anodizing, the voltage was increased at 0.2 V/s in the initial period until 50 V was reached and then the specimen was maintained at this voltage. A platinum plate (15 mm x 25 mm) was used as the counter electrode, and the specimens were set in parallel 15 mm from the counter electrode. The anodic current during the re-anodizing was measured by a digital multimeter connected to a PC system, and the structural changes of the specimen were examined by scanning electron microscopy (SEM: Miniscope TM-1000, Hitachi). In the observations of the vertical cross-section, the specimens were embedded in epoxy resin and mechanically polished. The formation process of the localized porous type oxide is shown in Fig. 1. To compare the local anodizing behavior after laser irradiation with the usual anodizing behavior, 50 V constant voltage anodizing was carried out on electropolished aluminum plates (S = 7.2 cm^2) until the whole plate is oxidized.

3. RESULTS AND DISCUSSION

3.1 Effect of pore-sealing and immersion temperature on chemical dissolution resistance of oxide films in oxalic acid solution

Immersion of aluminum specimens covered with porous anodic oxide films in doubly-distilled boiling water causes the hydration of anodic oxide films via the following equation [15, 20-22].

$$Al_2O_3 + nH_2O = Al_2O_3\,nH_2O \qquad (1)$$

Equation 1 results in the sealing of pores with hydroxide due to the volume expansion. During immersion, most of the hydration occurs at the outermost part of the oxide film, where highly crystalline hydroxide layers are formed, and the thickness and crystallinity of the hydroxide increase with immersion time [9, 20, 23-27]. The insulating properties and resistance to chemical dissolution in acid and alkaline solutions of oxide films increase with pore-sealing time [15], and this will be described in terms of the time-variations in the rest potential of specimens during immersion in acid or alkaline solutions.

Fig. 2 shows the changes in the rest potential of the anodized and pore-sealed specimens, E_r, with immersion time, t_i, in 0.22 M $(COOH)_2$ solution at T_i = 293 K. Here, the anodizing conditions of all specimens were as described in 2.1 above, and pore-sealing was performed in doubly distilled water at 373 K for periods of t_p = 15 – 120 min. For the t_p = 15 min specimen, E_r indicates the value of -0.2 V (vs. sat. Ag/AgCl) at the initial stage up to t_i = 1.5 h, then drops with t_i to reach a steady value of about -0.8 V at t_i = 5 h. This steady value of the potential is almost the same as that observed for an aluminum specimen covered with air-formed oxide films [10]. Therefore, the curve suggests that the pore-sealed anodic oxide films dissolve gradually into the oxalic acid solution, and that the substrate is exposed through the thin oxide layer after 5 h of immersion [28, 29].

On specimens with t_p = 60 and 120 min, E_r gradually shifts to more positive potentials in the initial period, and then also decreases with immersion time like the t_p = 15 min specimen. The potential increase at the initial stage, which is caused by the improvement of the insulating properties of anodic oxide films, may be due to the progress of aging of the hydroxide. The subsequent potential drop is due to increases in the area of the substrate exposed to the solution through imperfections in the oxide film by oxide dissolution. In the immersion tests, both aging and dissolution of oxide take place, with the aging process being more prevalent than dissolution in the initial stage. This is because highly crystalline hydroxide at the outermost part of the pore-sealed oxide films disturbs the oxide dissolution. It is clear from Fig. 2 that the starting time of the E_r drop is longer for specimens with longer t_p. This comparison suggests that the chemical dissolution resistance of the anodic oxide films becomes higher with increasing pore-sealing time.

Fig. 3 shows E_r vs. t_i curves obtained at 280 K. The rest potential, E_r, of the specimen with t_p = 15 min rises initially and then, after a maximum at t_i = 8 h, drops

gradually with t_i. In contrast, the E_r of specimens with t_p = 60 and 120 min reaches a steady value at t_i = 15 h after an initial rise. The E_r value after t_i = 5 h is more positive for specimens with longer t_p. Comparing Figs. 2 and 3 suggests that the dissolution rate of pore-sealed oxide films strongly depends on the temperature of the immersion solution, with lower dissolution rates at lower temperatures. The pore-sealed oxide films may lose functionality as masks during re-anodizing in 0.22M-$(COOH)_2$ at 297 K, whereas this ability may be maintained with more than 24 h of re-anodizing at 280 K [30].

In the following experiments, specimens with t_p = 120 min were used for laser irradiation and re-anodizing, and the re-anodizing was carried out at 280 K after laser irradiation.

3.2 Growth of porous type oxide films after laser irradiation

Fig. 4 shows SEM images of (a) the surface and (b) a vertical cross-section of a laser-irradiated specimen at P = 1.0 mW and v = 33 μm/s. In Fig. 4a, the top and bottom gray parts correspond to the area remaining covered with anodic oxide films, and the central light gray part is the laser-irradiated area. It can be seen from Fig. 4a that a 35-μm wide band of oxide film is removed, and that the exposed aluminum substrate has an uneven surface due to rapid melting and solidification of the aluminum by the laser irradiation. The vertical cross-section of the laser-irradiated area across the laser-irradiated line is semicircular and 9 μm deep from the top of the oxide film (Fig. 4b) due to the Gaussian energy distribution of the laser beam. It is clear that the laser irradiation causes the etching of the substrate as well as film removal, without damaging the oxide film around the laser-irradiated line.

Fig. 5 shows the changes in anodic current, I_a, with anodizing and re-anodizing time, t_a, in a 0.22 M $(COOH)_2$ solution at 280 K using (a) an electropolished aluminum plate (anodizing area, S = 720 mm^2) and (b) a laser-irradiated specimen (S = 0.035 x 4 x 5 = 0.7 mm^2). In Fig. 5a, the I_a increases rapidly in the very initial period and maintains a steady value of 25 mA for 2 h before gradually decreasing with anodizing time up to t_a = 93 h. At t_a = 93 h, i_a decreases rapidly to zero because the aluminum substrate is almost completely oxidized. In contrast with the electropolished plate (Fig. 5a), the laser-irradiated specimen in Fig. 5b shows a linear increase in i_a with t_a after a sharp current peak at the initial transient, and there are three smaller bumps on the current-time curve at t_a = 8, 17, and 27 h (Fig. 5b). The current density of electropolished and laser-irradiated specimens at t_a = 2 h were calculated to be 34.7 (= 25 x 10^{-3} / 720 x 10^{-6}) and 14.3 (= 10 x 10^{-6} / 0.7 x 10^{-6}) A/m^2.

The behavior of both specimens after anodizing for long periods of time is explained below. In potentiostatic anodizing of electropolished specimens, porous oxide films grow at a steady rate due to a balance between oxide formation at the oxide/substrate interface and electrochemical dissolution of oxide at the pore bottom. The electrochemical dissolution rate is determined by the inward diffusion of H^+ and

oxalate ions through the solution in the pores [20, 31]. Therefore, potentiostatic anodizing results in a steady current, as shown at the initial stage before 2 h of anodizing in Fig. 5a. However, the supply of H^+ and oxalate ions to the pore bottom becomes more difficult as the porous layer becomes thicker, which suppresses the electrochemical dissolution and results in the current decrease as was observed at longer than 2 h of anodizing in Fig. 5a.

For the laser-irradiated specimen (Fig. 5b), where micro-areas of the substrate were exposed, the decrease in I_a in the first 1 h of re-anodizing may be due to a suppression of the supply of H^+ and oxalate ions by the narrow gate presented by the pore-sealed anodic oxide film used as a mask. This can be ascertained by the fact that the current density at t_a = 2 h on the laser-irradiated specimen is much smaller than that on electropolished one.

The I_a increase after t_a = 2 h on the laser-irradiated specimen is attributed to the increase in the area of the interface between the substrate and newly formed oxide during re-anodizing, as shown in Figs. 6 and 7. Fig. 6 shows a SEM image of the surface of a specimen re-anodized in $(COOH)_2$ solution for t_a = 72 h after the first anodizing and laser irradiation. Fig. 6 shows numerous cracks in the anodic oxide film around the laser-irradiated area, these cracks are parallel to the longitudinal direction of the laser-irradiated area. The top layers of the oxide films are removed partly in areas where cracks have formed, and this can be explained as the result of detachment of highly crystalline hydroxides formed on the anodic oxide film during pore-sealing. Fig. 7 shows SEM images of the vertical cross-section of re-anodized specimens for (a) t_a = 4, (b) 32, and (c) 72 h. The images were taken across the laser-scanned line. At the initial stage of re-anodizing, porous type oxide films grow on the concave-shaped surface formed by the laser irradiation, as shown Fig. 7a. Renshaw [32] and Takahashi [33] et al. have reported that radial oxide film growth occurs when aluminum covered with an oxide film involve imperfections is anodized in acid solutions. At t_a = 32 h (Fig. 7b), a semi-circular or parabolic-shaped oxide, 100 μm wide and 45 μm deep, is observed at the laser irradiated area. The top of the oxide appears to be a gently sloping mound with a shallow concave at the central part. The shallow concave corresponds to the one produced at the surface of the substrate by the laser irradiation. The porous type oxide described in Fig. 7b has a fan-shape in the intersection of laser-scanned line, and may have a pore-branching structure microscopically that is similar to that obtained by a previous study [32, 33]. The formation of the oxide mound is due to a high value of the Pilling-Bedworth ratio, R_{pb}, during re-anodizing, defined as the ratio of the volumes of oxide formed and the metal substrate consumed in oxidation. The R_{pb} depends on the anodizing conditions, showing R_{pb} = 1.2 – 1.65 in the formation of porous anodic oxide film by anodizing in acid solution [34]. This is the case in the present investigation, and the formation of the oxide mound can be explained as the result of an expansion of the specimen volume.

It can be seen from Fig. 7b that oxide films formed by the first anodizing remain

on the surface except in the laser-irradiated area, and that there are several cracks in the oxide film over the semicircular oxide formed during the re-anodizing. The formation of cracks is easily understood to be due to the stress generated by the volume expansion. At t_a = 72 h (Fig. 7c), the semicircular or parabolic-shaped oxide is 170 μm wide and 85 μm deep, and the mound shaped, shallowly concave oxide is more pronounced than at 32 h. The anodic oxide film formed during the first anodizing still remains undissolved at t_a = 72 h, and more cracks are observed in the oxide film on the semicircular oxide. Formation of oxide films was not observed at areas that were not laser-irradiated even at t_a = 72 h, as suggested by Fig. 7c. This suggests good insulating properties of the pore-sealed oxide film formed in $(COOH)_2$ solution. Fig. 7d shows a high magnification image of Fig. 7c at the interface between the oxide film and aluminum substrate. It is clear that there is porous type oxide at the laser-irradiated area, and the pores in the oxide have 50 – 70 nm diameter. The average of cell size, D_c, indicates D_c = 145 nm, and the density of pore calculated from the cell size is 1.9 x 10^{14} m^{-2}. These values of pore diameter and cell size are slightly larger than those reported in the literatures [35-37].

As shown in Fig. 7, the interface between the semicircular oxide films and the aluminum substrate shows an arc of a circle and becomes longer with longer re-anodizing time, t_a. Fig. 8 shows the changes in the length of the interface, L, with t_a. The L value increases linearly with t_a from L = 50 μm at 2 h to L = 250 μm at 72 h. The linear increase in L with t_a after 2 h during re-anodizing (Fig. 8) should be correlated with the linear increase in I_a (Fig. 5b), since the total area of the oxide / substrate interface for current flow during re-anodizing can be expressed as L x l x n, and thus proportional to L. The proportionality constant in I_a vs. t_a, however, curves between 2 and 72 h, which is about 2.5, is different from that in the L vs. t_a curve, which is about 5.0. This can be explained by the stronger suppression of H^+ and oxalate ions in the thicker oxide films, as explained above for the anodizing of electropolished specimens (see Fig. 5a).

The small bumps in the I_a vs t_a curve for the re-anodizing (Fig. 5b) are related to the formation of cracks in the oxide film formed in the initial anodizing (Fig. 7). Fig. 9 shows high magnification SEM images of the vertical cross-section of a specimen re-anodized for 72 h, focused on the area where there are three interfaces between planar oxide films / the substrate, planar oxide film / semicircular oxide film, and semicircular oxide film / the aluminum substrate. Fig. 9a was taken at the same position of the specimen as Fig. 9b, but the pretreatments for the observation were different: no etching in Fig. 9a and etching in 4.2 M NaOH / 0.25 M $K_3[Fe(CN)_6]$ solution for 20 s in Fig. 9b. In Fig. 9a, there is a crack penetrating throughout the planar oxide film, and a gray, semicircular 10-μm diameter part is observed in the substrate phase at the bottom of the crack. The image obtained after etching reveals that the semicircular column oxide grows radially from the laser-irradiated area, and that the small semicircular part at the bottom of the crack in Fig. 9a corresponds to the oxide formed by the penetration

of solution through the crack. The small bumps in the I_a vs. t_a curve during re-anodizing in Fig. 5b can be explained in terms of the semicircular oxide formation at the bottom of cracks.

Fig. 10 shows a schematic model of localized formation of porous type oxide films by anodizing, pore-sealing, laser irradiation, and re-anodizing. Semicircular shaped 35-μm wide and 9-μm deep grooves are formed by a pulsed Nd-YAG laser irradiation of aluminum covered with pore-sealed anodic oxide films (Fig. 10a). Porous anodic oxide films are formed at the laser-irradiated area by re-anodizing, and grow radially in the initial period to form a semi-circular column of oxide (Fig. 10b). Cracks develop in the planar pore-sealed oxide film around the laser-irradiated area, due to stresses generated by the formation of small mounds at the top of the semicircular columnar oxide, and this causes semicircular oxide to form at the bottom of the cracks (Fig. 10c). After long re-anodizing, relatively large semicircular columnar oxide grows underneath the pore-sealed anodic oxide films, causing the formation of further cracks in the oxide film around the laser-irradiated area (Fig. 10d).

In summary, porous type oxide films were successfully formed at selected micro-areas by the successive steps of anodizing, pore-sealing, laser irradiation, and re-anodizing, although many cracks were formed in the pore-sealed oxide film around the area. To avoid crack formation, anodizing conditions with low values of the Pilling-Bedworth ratio should be chosen. Low R_{pb} values can be obtained by anodizing with low current density and in Ematal solution containing potassium titanium oxalate [38]. Further investigation of the formation of the anodic oxide films at selected micro-areas with no cracking should be done in order to apply this technique in the micro- and nano-technology.

4. CONCLUSIONS

The following conclusions may be drawn from the investigation on local anodizing at micro-areas by the successive steps of anodizing, pore-sealing, laser irradiation, and re-anodizing.

(1) Pore sealing in doubly-distilled boiling water for 120 min after anodizing of aluminum gives rise to a considerable improvement of the insulating properties of the anodic oxide film, showing a potential function similar to masks, for up to 72 h in a $(COOH)_2$ solution at 280 K.

(2) Porous anodic oxide film grows radially at the laser-irradiated area, to form semicircular columnar oxide generating a small mound at the top of the oxide. Many cracks are formed in the pore-sealed oxide film around the laser-irradiated area due to stresses generated by the mound formation.

Acknowledgements

The research was supported by a Grant-in-Aid from the Ministry of Education, Culture, Sports, Science and Technology, Japan. The authors are indebted to Dr. K.

Ebihara, Nippon Light Metals Co. for supplying the aluminum plate. The authors are also indebted to Dr. Hyono, Hokkaido University for FE-SEM observation.

References

1) H. Masuda and K. Fukuda, Science 268 (1995) 1466
2) H. Asoh, S. Ono, T. Hirose, M. Nakao, and H. Masuda, Electrochim. Acta 48 (2003) 3171
3) P. Evans, W. R. Hendren, R. Atkinson, G. A. Wurtz, W. Dickson, A. V. Zayats, and R. J. Pollard, Nanotechnology 17 (2006) 5746
4) T. Nagaura, F. Takeuchi, Y. Yamauchi, K. Wada, and S. Inoue, Electrochem. Commun. 10 (2008) 681
5) E. C. Vermisoglou, G. Pilatos, G. E. Romanos, G. N. Karanikolos, N. Boukos, K. Mertis, N. Kakizis, and N. K. Kanellopoulos, Micropor. Mesopor. Mater. 110 (2008) 25
6) H. Jha, T. Kikuchi, M. Sakairi, and H. Takahashi, Nanotechnology 19 (2008) 395603
7) E. Perre, L. Nyholm, T. Gustafsson, P. L. Taberna, P. Simon, and K. Edstrom, Electrochem. Commun. 10 (2008) 1467
8) L. Zhixun, F. Yan, Z. Xiaofang, and Y. Jiannian, Mater. Chem. Phys. 107 (2008) 91
9) M. Lelonek and M. Knoll, Electrochim. Acta 53 (2008) 4818
10) S. Z. Chu, M. Sakairi, H. Takahashi, K. Shimamura, and Y. Abe, J. Electrochem. Soc. 147 (2000) 2181
11) T. Kikuchi, S. Z. Chu, S. Jonishi, M. Sakairi, and H. Takahashi, Electrochim. Acta 47 (2001) 225
12) T. Kikuchi, M. Sakairi, H. Takahashi, Y. Abe, and N. Katayama, J. Electrochem. Soc. 148 (2001) C740
13) T. Kikuchi, M. Sakairi, and H. Takahashi, J. Electrochem. Soc. 150 (2003) C567
14) Y. Akiyama, T. Kikuchi, M. Ueda, M. Iida, M. Sakairi, and H. Takahashi, Electrochim. Acta 51 (2006) 4834
15) T. Kikuchi, H. Takahashi, and T. Maruko, Electrochim. Acta 52 (2007) 2007
16) T. Kikuchi, Y. Akiyama, M. Ueda, M. Sakairi, and H. Takahashi, Electrochim. Acta 52 (2007) 4480
17) H. Jha, T. Kikuchi, M. Sakairi, and H. Takahashi, J. Micromech. Microeng. 17 (2007) 1949
18) H. Jha, T. Kikuchi, M. Sakairi, and H. Takahashi, Electrochim. Acta 52 (2007) 4724
19) M. Sakairi, M. Yamada, T. Kikuchi, and H. Takahashi, Electrochim. Acta 52 (2007) 6268
20) M. Koda, H. Takahashi, and S. Nagayama, J. Surf. Finish. Soc. Jpn. 33 (1982) 242
21) J. P. Hoar and G. C. Wood, *Electrochim. Acta* 7 (1962) 333
22) J. P. O'Sullivan and G. C. Wood, *J. Electrochem. Soc.*, 116 (1969) 1351
23) K. Wefers, *Aluminum*, 49 (1973) 622
24) M. Koda, H. Takahashi, and M. Nagayama, *J. Surf. Fin. Soc. Jpn.,* 33 (1982) 460
25) M. Koda, H. Takahashi, and M. Nagayama, *J. Surf. Fin. Soc. Jpn.,* 33 (1982) 614

26) M. Koda, H. Takahashi, and M. Nagayama, *J. Surf. Fin. Soc. Jpn.,* 34 (1983) 44
27) H. Jha, T. Kikuchi, M. Sakairi, and H. Takahashi, *Electrochim. Acta*, 52 (2007) 4724
28) J. R. Davis, Corrosion of Aluminum and Aluminum Alloy, ASM International, OH, 1999
29) M. Pourbaix, Atlas of Electrochemical Equilibria in Aqueous Solutions, National Association of Corrosion Engineers, TX, 1974
30) S. Wernick, R. Pinner, and P. G. Sheasby, The Surface Treatment and Finishing of Aluminum and Its Alloys, 4th ed., Finishing Publications, England, 1987
31) M. Koda, H. Takahashi, and S. Nagayama, J. Surf. Finish. Soc. Jpn. 28 (1977) 584
32) T. A. Renshaw, J. Electrochem. Soc., 108 (1961) 185
33) H. Takahashi, M. Nagayama, H. Akahori, and A. Kitahara, J. Electron Microscopy 22 (1973) 149
34) S. J. Garcia-Vergara, P. Skeldon, G. E. Thompson, and H. Habazaki, Electrochim. Acta 52 (2006) 681
35) K. Ebihara, H. Takahashi, and M. Nagayama, J. Surf. Finish. Soc. Jpn. 33 (1982) 156
36) K. Ebihara, H. Takahashi, and M. Nagayama, J. Surf. Finish. Soc. Jpn. 34 (1983) 548
37) K. Ebihara, H. Takahashi, and M. Nagayama, J. Surf. Finish. Soc. Jpn. 35 (1984) 205
38) S. Ono and T. Sato, J. Metal Finish. Soc. Jpn 31 (1980) 134

Captions

Fig. 1 Schematic model of the steps in the formation of localized porous type oxide films: (a) anodizing, (b) pore-sealing, (c) laser irradiation, and (d) re-anodizing.

Fig. 2 Changes in the rest potential of anodized specimens, E_r, with immersion time, t_i, in a 0.22 M $(COOH)_2$ solution at 293 K. Anodizing was carried out in a 0.22 M $(COOH)_2$ solution at 293 K for 10 min with a constant current density of 100 A/m^2, and pore sealing was by immersing in doubly-distilled boiling water for different t_ps.

Fig. 3 Changes in the rest potential of anodized specimens, E_r, with immersion time, t_i, in a 0.22 M $(COOH)_2$ solution at 280 K. Conditions of anodizing and pore sealing are as in Fig. 2

Fig. 4 SEM images of (a) surface and (b) cross-section of pore-sealed specimen after laser irradiation. Anodizing conditions as in Fig. 2, and pore sealing was carried out by immersing in doubly-distilled boiling water for 120 min. Laser irradiation was carried out in doubly distilled water at 295 K, using a pulsed Nd-YAG laser with 532 nm wavelength, 8 ns pulse width, and 10 Hz frequency at a 33 μm/s scanning rate.

Fig. 5 Changes in the anodic current, I_a, with anodizing time, t_a, in a 0.22 M $(COOH)_2$ solution at 280 K using (a) electropolished aluminum plate (surface area: 720 mm^2) and (b) a laser-irradiated specimen (0.7 mm^2). The laser-irradiated specimen had anodizing, pore-sealing, and laser-irradiation conditions as in Figs. 3 and 4.

Fig. 6 SEM image of the surface of specimen re-anodized in a 0.22 M $(COOH)_2$ solution at 280 K for 72 h after anodizing, pore-sealing, and laser-irradiation. Conditions of pretreatments before re-anodizing are as Fig. 6.

Fig. 7 SEM images of the cross-section of specimens re-anodized in a 0.22 M $(COOH)_2$ solution at 280 K for (a) 4 h, (b) 32 h, and (c, d) 72 h after anodizing, pore-sealing and laser-irradiation. The image was obtained by exposing the specimen across a laser scanned line, and conditions of pretreatments before re-anodizing are as Fig. 6.

Fig. 8 Time-variations in the length, L, of the semicircular anodic oxide / aluminum substrate interface across the laser scanned line substrate during re-anodizing in a 0.22 M $(COOH)_2$ solution at 280 K.

Fig. 9 High magnification SEM images of the cross-section of specimen re-anodized in a 0.22 M $(COOH)_2$ solution at 280 K for 72 h after anodizing, pore-sealing and laser-irradiation. Both images show the same region, but preparations for the observations were different: (a) no etching and (b) chemical etching.

Fig. 10 Schematic models of the growth of the localized anodic oxide film: (a) film removal by laser irradiation, (b) growth of oxide film at the laser-irradiated area, (c) radial growth of semicircular columnar oxide around the laser-irradiated area, formation of cracks, and oxide formation under the cracks, and (d) formation of large semicircular columnar oxide with a small mound.

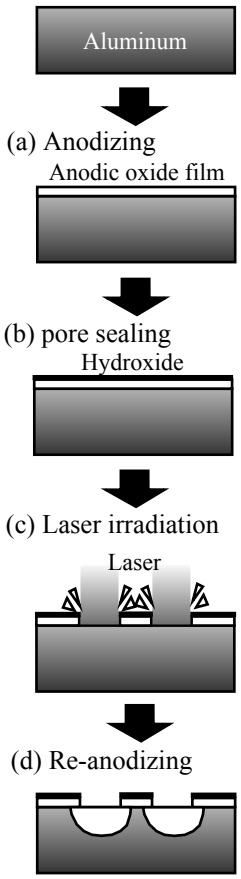
Aluminum
(a) Anodizing
Anodic oxide film
(b) pore sealing
Hydroxide
(c) Laser irradiation
Laser
(d) Re-anodizing

Fig. 1

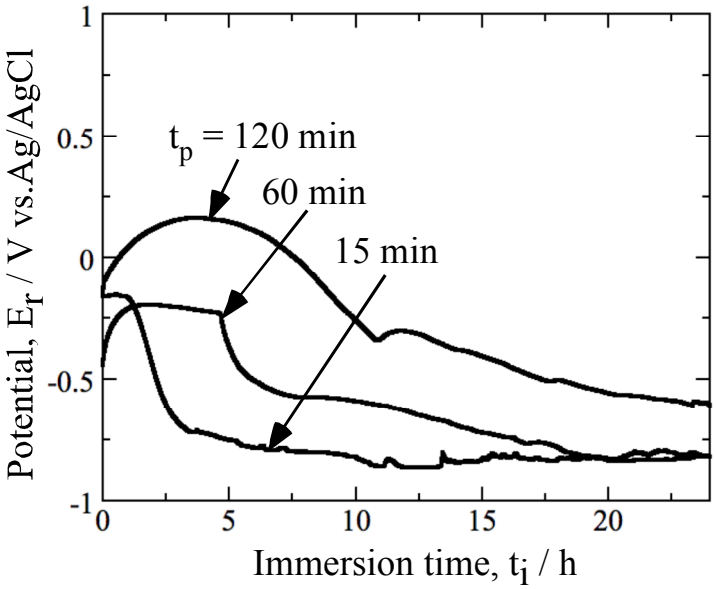
1
0.5
0
-0.5
-1
0
5
10
15
20
t_p = 120 min
60 min
15 min
Potential, E_r / V vs.Ag/AgCl
Immersion time, t_i / h

Fig. 2

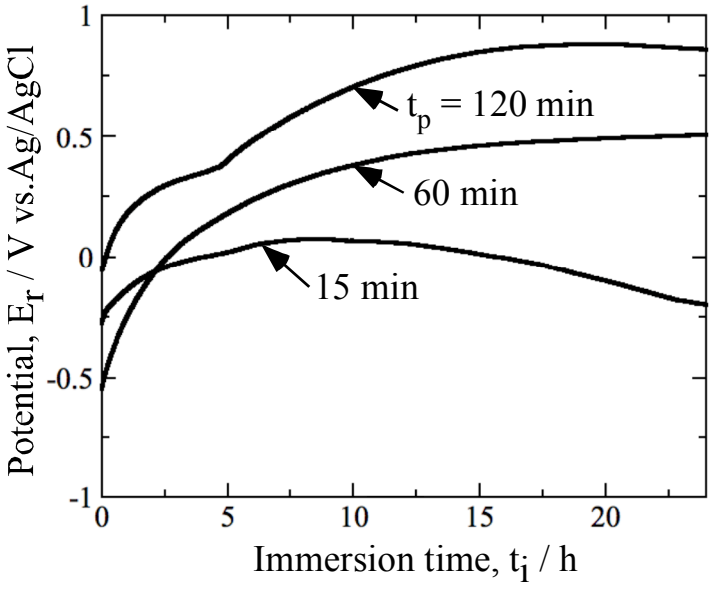
Potential, E_r / V vs.Ag/AgCl
Immersion time, t_i / h
t_p = 120 min
60 min
15 min
1
0.5
0
-0.5
-1
0
5
10
15
20

Fig. 3

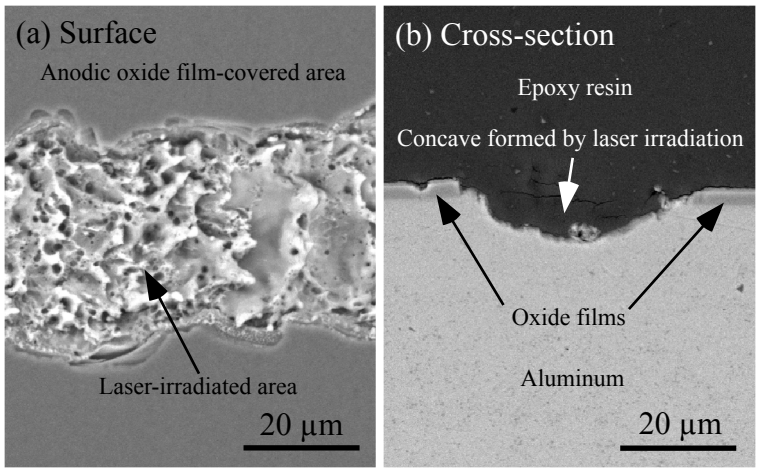
(a) Surface
Anodic oxide film-covered area
Laser-irradiated area
20 μm
(b) Cross-section
Epoxy resin
Concave formed by laser irradiation
Oxide films
Aluminum
20 μm

Fig. 4

(a) Aluminum plate

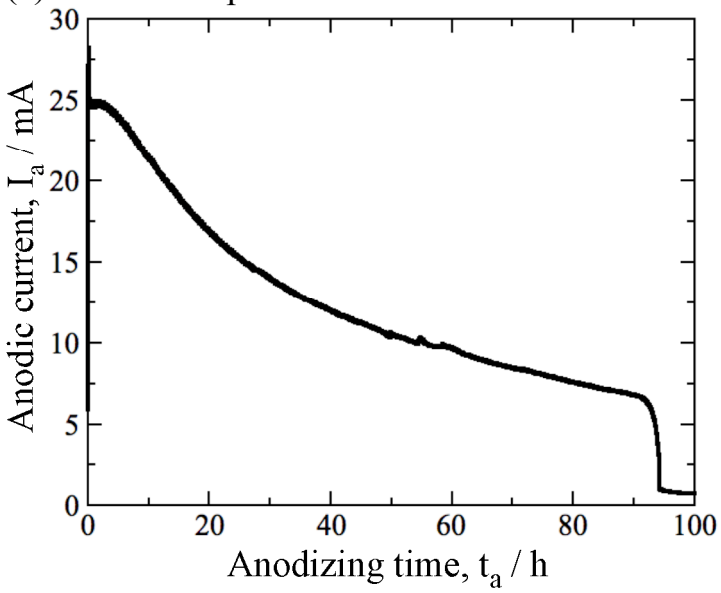

(b) Laser-irradiated specimen

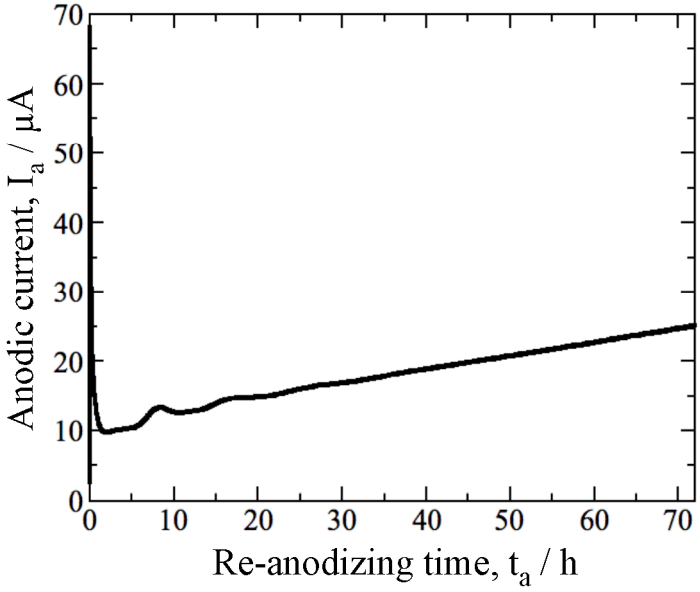

Fig. 5

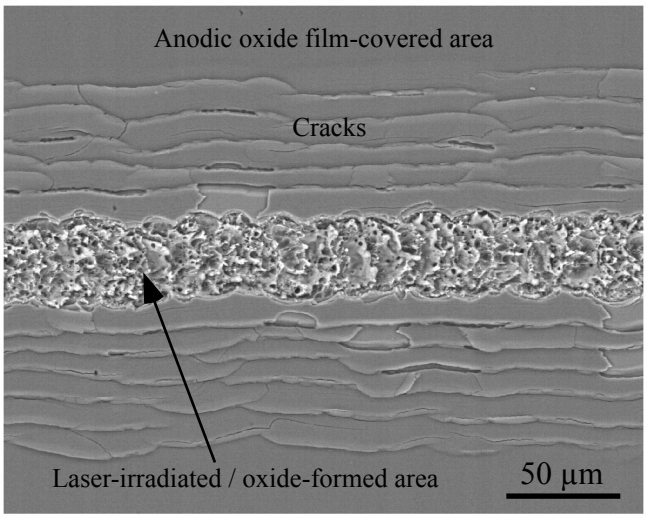
Anodic oxide film-covered area
Cracks
Laser-irradiated / oxide-formed area
50 μm

Fig. 6

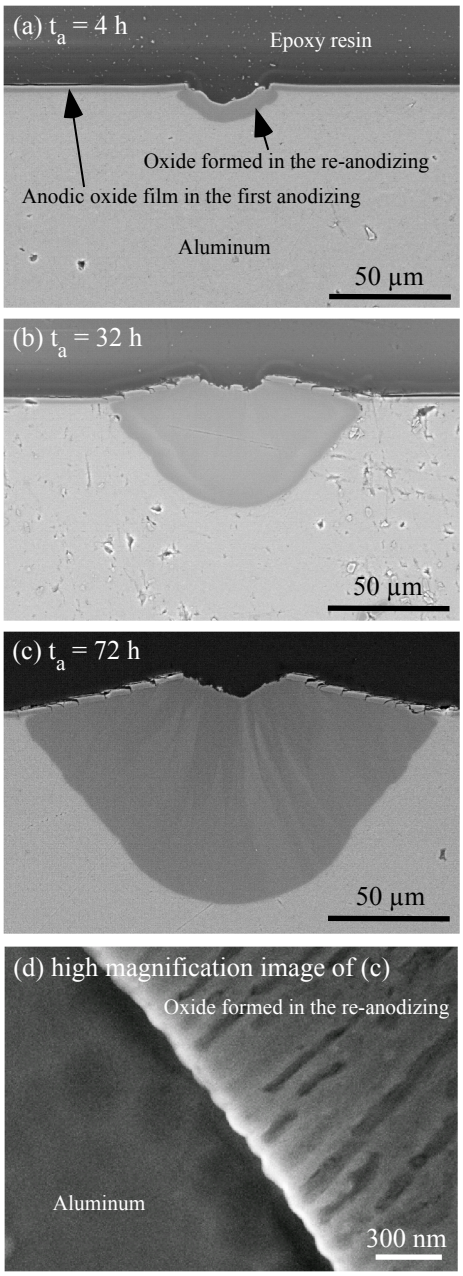
(a) t_a = 4 h
Epoxy resin
Oxide formed in the re-anodizing
Anodic oxide film in the first anodizing
Aluminum
50 μm
(b) t_a = 32 h
50 μm
(c) t_a = 72 h
50 μm
(d) high magnification image of (c)
Oxide formed in the re-anodizing
Aluminum
300 nm

Fig. 7

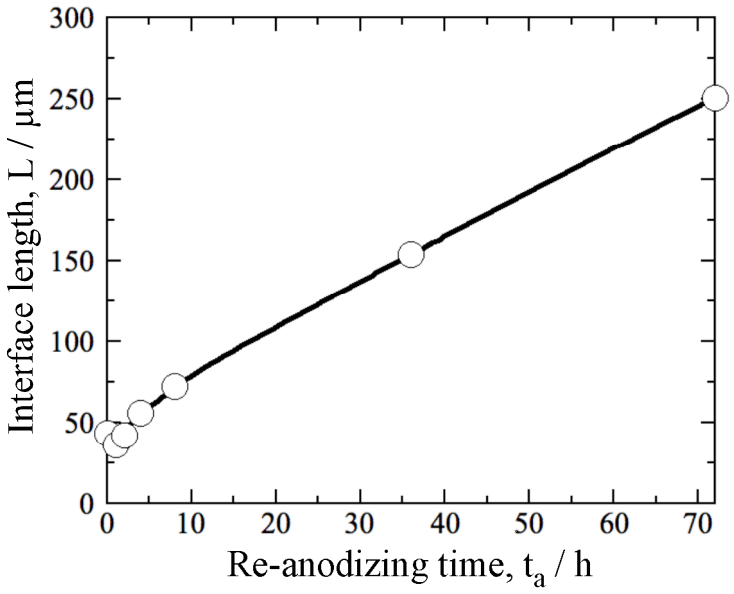
Interface length, L / μm
300
250
200
150
100
50
0
0
10
20
30
40
50
60
70
Re-anodizing time, t_a / h

Fig. 8

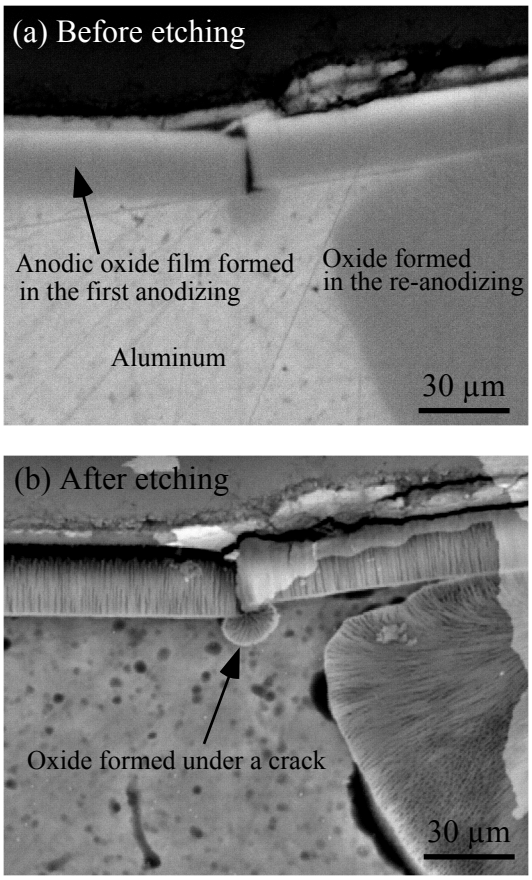
(a) Before etching
Anodic oxide film formed
in the first anodizing
Oxide formed
in the re-anodizing
Aluminum
30 μm
(b) After etching
Oxide formed under a crack
30 μm

Fig. 9

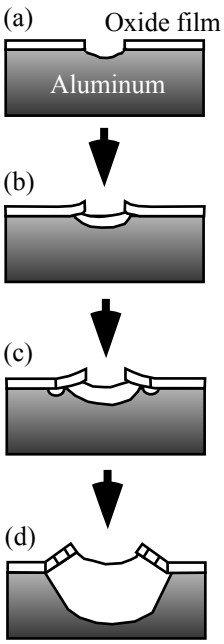

Fig. 10